ACCEPTED VERSION

Todero Peixoto, Carlos Jose; de Souza, Victor; Bellido Caceres, Jose Alfredo
Comparison of the moments of the X(max) distribution predicted by different cosmic ray shower simulation models

---

PERMISSIONS

http://www.elsevier.com/journal-authors/policies/open-access-policies/article-posting-policy#accepted-author-manuscript

16 October 2013

---

http://hdl.handle.net/2440/79804

Comparison of the moments of the X_{max} distribution predicted by different cosmic ray shower simulation models

Carlos Jose Todero Peixoto[a], Vitor de Souza[a], Jose Bellido[b]

[a]*Instituto de Física de São Carlos, Universidade de São Paulo, Brazil.*
[b]*University of Adelaide, Adelaide, S.A. 5005, Australia.*

Abstract

In this paper we study the depth at which a cosmic ray shower reaches its maximum (X_{max}) as predicted by Monte Carlo simulation. The use of X_{max} in the determination of the primary particle mass can only be done by comparing the measured values with simulation predictions. For this reason it is important to study the differences between the available simulation models. We have done a study of the first and second moments of the X_{max} distribution using the CORSIKA and CONEX programs. The study was done with high statistics in the energy range from 10^{17} to $10^{20.4}$ eV. We focus our analysis in the different implementations of the hadronic interaction models SIBYLL2.1 and QGSJETII in CORSIKA and CONEX. We show that the predictions of the $\langle X_{max} \rangle$ and RMS(X_{max}) depend slightly on the combination of simulation program and hadronic interaction model. Although these differences are small, they are not negligible in some cases (up to 5 g/cm^2 for the worse case) and they should be considered as a systematic uncertainty of the model predictions for $\langle X_{max} \rangle$ and RMS(X_{max}). We have included a table with the suggested systematic uncertainties for the model predictions. Finally, we present a parametrization of the X_{max} distribution as a function of mass and energy according to the models SIBYLL2.1 and QGSJETII, and showed an example of its application to obtain the predicted X_{max} distributions from cosmic ray propagation models.

Keywords: Composition, Monte Carlo Simulation, Hadronic Interaction Models

1. Introduction

The cosmic ray composition at the highest energies is probably the most difficult and most meaningful question yet to be solved in the present astroparticle physics scenario. Due to the unknown strength and structures of the magnetic fields in the Universe, anisotropy studies are also intrinsically dependent on the mass composition and a better identification of the sources is probably only going to be possible if the cosmic ray composition is known beforehand.

The most reliable technique to infer the mass composition of showers with energy above 10^{17} eV is the determination of the X_{max} and posterior comparison of the measured values with predictions from Monte Carlo simulation. This is because above 10^{17} eV fluorescence detectors can measure X_{max} with a resolution of 20 g/cm^2. The evolution of the detectors, the techniques used to measure the atmosphere, the advances in the understanding of the fluorescence emission and the development of innovative analysis procedures have resulted in a high precision measurement of X_{max} and its moments. The Pierre Auger Observatory [3], the HiRes Experiment [4], the Telescope Array [5] and the Yakutsk array [6] quote systematic uncertainties in the determination of the $\langle X_{max} \rangle$ to be 12, 3.3, 15 and 20 g/cm^2, respectively. Considering the quoted errors and taking into account that the data have to be compared to simulation predictions, it is very important to understand the details and reduce the differences between simulation programs. The proposed experiment JEM-EUSO [7] is also going to use the fluorescence technique to detect air shower from the space. For this reason, we extended the analysis done in this work up to $10^{20.4}$ eV within the energy range aimed by JEM-EUSO.

The dependency of X_{max} with primary energy and mass (A) has been analytically studied in a hadronic cascade model [9]. Monte Carlo programs can simulate the hadronic cascade in the atmosphere using extrapolation from the measured hadronic cross sections at somewhat lower energy. It has been shown before that different hadronic interaction models do not agree in the prediction of the $\langle X_{max} \rangle$ and other parameters [10].

In this paper we study in detail the dependence of $\langle X_{\max} \rangle$ and $\mathrm{RMS}(X_{\max})$ as a function of energy and primary mass. We compare the result of two hadronic interaction models. We have done a high statistics study and we show that the discrepancies between models and programs are at the same level of quoted systematic uncertainties of the experiments. The analysis done here points to the need of a better understanding of the interaction properties at the highest energies which can be achieved by ongoing analysis of the LHC data which already resulted in updates of the hadronic interaction models. At the same time the results presented in this paper point to discrepancies between different implementations of the same hadronic interaction model which need to be better understood.

We also present a parametrization of the $X_{\max}$ distribution as a function of mass and energy. Several theoretical models have predicted the mass abundance based on astrophysical arguments [11, 12, 13, 14]. In order to compare the predicted abundance with measurements, one has to convert the calculated flux for each particle into $X_{\max}$. Until now, this could only be done using full Monte Carlos simulations. We present here a parametrization of the $X_{\max}$ distribution to allow the conversion of astrophysical models into $X_{\max}$ measurements. Parametrizations of $\langle X_{\max} \rangle$ as a function of energy and mass have been already studied [9]. What we present here is a step forward, we show the parametrization of the $X_{\max}$ distribution which is good enough to calculate the first and second moments of the distribution.

In section 2, we study the dependence of the results regarding simulation limitations like thinning and nucleon types. In section 3, we compare the models. In Section 4 we show the parametrization of the $X_{\max}$ distribution. Section 5 concludes our analysis.

2. Shower Simulation

In this work we have used CONEX [15, 16] and CORSIKA [17] shower simulators. CONEX uses a one dimensional hybrid approach combining Monte Carlo simulation and numerical solutions of cascade equations. CORSIKA describes the interactions using a full three dimensional Monte Carlo algorithm. By using analytical solutions, CONEX saves computational time. On the other hand, CORSIKA makes use of the thinning algorithm [18, 19] to reduce simulation time and output size.

Both approaches have negative and positive features. CORSIKA offers a full description of the physics mechanisms and a three dimensional propagation of the particles in the atmosphere. However, it is very time consuming, limiting studies which depend on large number of events at the highest energies. The thinning algorithm introduces spurious fluctuations that have to be taken into account in the final analysis. CONEX is fast, but on the other hand it offers only a one dimensional description of the shower. The use of intermediate analytical solutions might also reduce the intrinsic fluctuation of the shower. In the following sections both programs are compared in detail concerning the $X_{\max}$ calculations.

The hadronic interaction models for the highest energies were developed independently of the programs that describe the showers. For each shower simulator many hadronic interaction models are available. We have used QGSJETII.v03 [20, 21] and SIBYLL2.1 [22] in this work. For the low energy hadronic interaction we have used GHEISHA [23] in all simulations.

Showers have been simulated with primary energy ranging from $10^{17.0}$ to $10^{20.4}$ eV in steps of $\log_{10}(E/eV) = 0.1$. We have simulated seven primary nuclei types with mass: 1, 5, 15, 25, 35, 45 and 55. For each primary particle, primary energy, and hadronic interaction model combination, a set of 1000 showers has been simulated. The zenith angle of the shower was set to 60° and the observation height was at sea level corresponding to a maximum slant depth of 2000 g/cm² allowing the simulation of the entire longitudinal profile of the showers. The longitudinal shower profile was sampled in steps of 5 g/cm². The energy thresholds in CORSIKA and CONEX were set to 1, 1, 0.001 and 0.001 GeV for hadron, muons, electrons and photons respectively.

2.1. Fitting the longitudinal development of the shower

For all studies in this paper, $X_{\max}$ was calculated by fitting a Gaisser-Hillas [24] function to the energy deposited by the particle through the atmosphere. We chose a four parameter Gaisser-Hillas (GH4) function given by:

$$\frac{dE}{dX}(X) = \frac{dE}{dX}^{max} \left(\frac{X - X_0}{X_{\max} - X_0} \right)^{\frac{X_{\max} - X_0}{\lambda}} \exp\left(\frac{X_{\max} - X}{\lambda} \right) \tag{1}$$

in which $\frac{dE}{dx}^{max}$, X_0, λ and X_{max} are the four fitted parameters and X is the slant atmospheric depth. The first guess of the X_{max} parameter in the fitting procedure was chosen to be the maximum of a three degree polynomial interpolated within the three points in the longitudinal profiles with largest $\frac{dE}{dX}$. The full simulated profile was fitted.

We have studied the effect of fitting a different function to the longitudinal profile. Instead of a Gaisser-Hillas function with four parameters, we have also fitted a Gaisser-Hillas function with 6 parameters (GH6). In this function, λ is defined as $\lambda = a \times X^2 + b \times X + c$ in which a, b and c are also fitted. The differences in X_{max} and RMS(X_{max}) calculations for both fitted functions were smaller than 2.5 g/cm^2 and 0.6 g/cm^2, respectively. Anyway, there might be a systematic effect in the determination of the X_{max} due to the fitting procedure and the fitted function chosen to describe the longitudinal profile, which is not investigated in this paper.

2.2. Thinning analysis

In order to save time and output size, CORSIKA uses a thinning algorithm [18, 19]. The thinning factor f_{thin} defines the fraction of the primary particle energy E_0 below which not all particles in the shower are followed. Particles with energy below E_{cut}, where $E_{cut} = f_{thin} * E_0$, are sampled, some are discarded and others followed. Each active particle in CORSIKA has a weight attribute which compensates for the energy of the rejected ones such as that energy is conserved.

The thinning algorithm causes artificial fluctuations in the calculation of the shower development which needs to be taken into account. For example, figure 1 shows the longitudinal development of one shower simulated with three thinning factors 10^{-5}, 10^{-6} and 10^{-7}. The first interaction altitude was fixed at 60 km and the target is Nitrogen nuclei. SIBYLL2.1 was used for this study. It illustrates how the fluctuations of the simulated longitudinal profile increase with increasing thinning factor.

Figure 2 shows the X_{max} distribution for 1000 simulated shower for three thinning factors. In this example the first interaction point and target were not fixed. SIBYLL2.1 was used again for this study. Figure 2 shows that the $\langle X_{max} \rangle$ and RMS(X_{max}) are very similar for any thinning factor used. The maximum difference is 0.4 g/cm^2 for $\langle X_{max} \rangle$ and 2.8 g/cm^2 for RMS(X_{max}). Based on this study we chose to simulate all showers with thinning factor 10^{-5}.

2.3. Isobaric Nuclei Analysis

Some of the simulation used in this paper have been produced for another study and have been re-used in this work to save computational time. The previously simulated showers have exotic primary particle with unstable number of protons and neutrons. In this section we compare the longitudinal development of showers started with exotic nuclei with the shower started with stable nuclei with the same total number of nucleons. Our intention is to show that the development of a shower at high energies does not depend on the number of protons and neutrons independently but depends only on the total number of nucleons considered.

CORSIKA and CONEX simulators differentiate isobaric nuclei by allowing the determination of the number of protons and neutrons of the primary nuclei. However the treatment of the first interaction is done by the hadronic interaction models. QGSJETII does not differentiate isobaric nuclei interactions, SIBYLL2.1 does differentiate.

At the highest energies the energy loss of protons and neutrons is negligible when compared to the total energy and therefore only the total number of nucleons should influence the development of the shower. On the other hand, Coulomb dissociation should also be taken into account [25]. Nevertheless, none of the hadronic interaction models available include this effect and therefore the development of the simulated shower should not depend on the number of protons and neutrons in the nuclei.

Figure 3 shows the X_{max} distribution for 10^{19} eV showers. We have simulated nuclei with different numbers of proton and neutron constituents. We can conclude that, at the energy range of interest, the predicted $\langle X_{max} \rangle$ and the RMS(X_{max}) does not depend on the number of protons and neutrons which form a nucleus with given mass A. The maximum difference in the $\langle X_{max} \rangle$ was 2.9 g/cm^2 for A = 24 and QGSJETII and in the RMS(X_{max}) was 2.5 g/cm^2 for A = 1 and SIBYLL2.1.

3. Results

Figures 4 and 5 show the comparisons of $\langle X_{max} \rangle$ using both simulators for SIBYLL2.1 and QGSJETII respectively. Figures 4e and 4f show the difference between CORSIKA and CONEX predictions as a function of energy and mass

respectively when both programs used Sibyll2.1. The same is shown in figures 5e and 5f for QGSJetII. The differences between the $\langle X_{\max} \rangle$ predicted by Corsika and Conex are smaller than 7 g/cm^2 in the parameter space studied by us. Conex tends to simulate showers slightly deeper than Corsika.

Similar results are presented in figures 6 and 7 for the RMS($X_{\max}$). In the parameter space studied by us the differences in the RMS($X_{\max}$) calculated by Corsika and Conex are smaller than 8 g/cm^2. No significant trend of the difference with energy or mass was seen.

The evolution of RMS($X_{\max}$) shown in figure 6a, 6b, 7a and 7b shows large fluctuations apparently larger than the estimated statistical fluctuation. The statistical fluctuation shown as error bars of RMS($X_{\max}$) is the standard statistical variance of the variance of a distribution. No Gaussian approximation was used. The trend of RMS($X_{\max}$) with energy is statisticaly incompatible with a linear behavior. A linear fit of RMS($X_{\max}$) versus energy shows a mean $\chi^2/NDOF = 123/35 \sim 3.5$.

Figure 8 summarizes the differences in $\langle X_{\max} \rangle$ and RMS($X_{\max}$) between the simulation programs and between the hadronic interaction models. This figure shows simultaneously the $\langle X_{\max} \rangle$ and RMS($X_{\max}$) values, where the corresponding $\langle X_{\max} \rangle$ and RMS($X_{\max}$) for a nuclei with mass 55 has been taken as reference (as suggested in [26]). This figure illustrates the importance of taking into account the simulation program differences into the systematic uncertainty of the model predictions. Each blob corresponds to the $\langle X_{\max} \rangle$ and RMS($X_{\max}$) predictions for one primary particle at different energies.

The elongation rate theorem [27, 28, 29] proposes the use of the slope of the variation of $\langle X_{\max} \rangle$ with energy as a composition parameter. According to this proposal, changes in this slope represents changes in composition. Figure 9 show the slope of the variation of $\langle X_{\max} \rangle$ and RMS($X_{\max}$) with energy as a function of primary particle mass for Corsika and Conex using Sibyll2.1 and QGSJetII. The slope in this figure corresponds to the fit of a straight line in the energy range ($10^{17} \leq E \leq 10^{20.4}$ eV). There is a good agreement between Conex and Corsika when the same hadronic model is used. The slope of the RMS($X_{\max}$) when Sibyll2.1 is used presents the largest discrepancy between Conex and Corsika (see 9.c).

It has been shown before [30] that the dependencies of the $\langle X_{\max} \rangle$ and RMS($X_{\max}$) are not strictly straight lines however the departure of the linear dependency is very small for energies above 10^{17} eV as studied here.

It is clear from figure 9 that the slope of the $\langle X_{\max} \rangle$ as a function of energy is dominated by the hadronic interaction model rather than by the shower simulation.

4. Parametrization of the $X_{\max}$ distributions

The $X_{\max}$ distributions can be described by a function which is a convolution of a Gaussian with an exponential [31]:

$$\frac{dX_{\max}}{dN} = N_f \exp\left(\frac{t_0 - t}{\lambda} + \frac{\sigma^2}{2\lambda^2}\right) Erfc\left(\frac{t_0 - t + \sigma^2/\lambda}{\sqrt{2}\sigma}\right) \tag{2}$$

This equation has four parameters. N_f is a normalization factor which gives the total number of events in the $X_{\max}$ distribution. λ, t_o and σ are parameters which are related to the decay factor of the exponential, the maximum of the distribution and the width of the distribution respectively. $Erfc$ is the error function. We used this equation to fit the $X_{\max}$ distributions of all mass and energies we have simulated. Figure 14 shows examples $X_{\max}$ distributions we fit with this equation. The aim of this study is to use equation 2 to fit the $X_{\max}$ distribution and calculate the $\langle X_{\max} \rangle$ and RMS($X_{\max}$). We show below that a convolution of a Gaussian with an exponential allows a good description of the $\langle X_{\max} \rangle$ and RMS($X_{\max}$). The proposed function is also a fairly good description of the $X_{\max}$ distribution, see figures 14.

After that, we parametrized λ, t_o and σ as a function of primary mass and energy using the simulated showers. Figure 10 show the evolution of the three parameters with energy and mass.

Figure 10a shows how t_o has a very smooth dependence with mass and energy, recovering the already explored dependence of $X_{\max}$ with mass and energy. On the other hand, σ and λ are not completely independent parameters. Both parameters influence the width of the $X_{\max}$ distribution in different ways. The parameter λ changes the width of the $X_{\max}$ distribution by modifying the decays of the exponential, making the high $X_{\max}$ tail longer or shorter. σ also changes the width of the $X_{\max}$ distribution by modifying the width of the central part. In fact, note that mathematically RMS($X_{\max}$) = $\sqrt{(\sigma + \lambda)}$.

4

Given the degeneracy in shaping the width of the X_{max} distribution, the parameters σ and λ are inversely correlated. The parameters σ and λ compensate each other, fluctuations to higher values of σ are correlated to fluctuations to smaller values of λ.

We performed a fit to plots in figure 10 with a linear dependence on $log_{10}(A)$ and $log_{10}(E)$ following equation:

$$\left.\begin{array}{c} t_0 \\ \sigma \\ \lambda \end{array}\right\} = C_1 \times log_{10}(E/eV) + C_2 \times log_{10}(A) + C_3 \tag{3}$$

Tables 1 and 2 show the fitted parameters for CONEX and CORSIKA respectively. Despite the fluctuations of σ and λ a linear fit in $log_{10}(A)$ and $log_{10}(E)$ is reasonably good approximation to describe the X_{max} distribution. This can be seen in figures 11 and 12 where we show a comparison between the simulation, the direct fit of the X_{max} distribution using equation 2 and the calculation using equation 3 and table 1.

It is clear that a direct fit of the X_{max} distributions with equation 2 (blue lines) leads to a very good description of the first and second moments of the X_{max} distribution. For all simulations and hadronic models in the entire energy range and for all primary particle used in our study the direct fit resulted in a difference on the simulation smaller than 2 g/cm^2 for $\langle X_{\text{max}} \rangle$ and smaller than 4 g/cm^2 in the RMS(X_{max}).

The fit to a plane $log_{10}(A)$ and $log_{10}(E)$ is a reasonably good approximation to describe the X_{max} distributions. This can be seen in figures 11 and 12 where we show a comparison between the simulation, the direct fit of the X_{max} distribution using equation 2 and the calculation using equation 3 and table 1.

The parametrization as a function of energy and mass of the parameters that describe the Xmax distributions (equation 3) introduced some systematic errors in $\langle X_{\text{max}} \rangle$ for the case of QGSJetII model (up to 10 g/cm^2). This is shown with red lines in figure 11 (right hand side plots). The reason for this systematic errors is because the parametrization used (equation 3) is not the optimum one for QGSJetII model.

	Had. Model	C_1 ($\pm$ err)	C_2 ($\pm$ err)	C_3 ($\pm$ err)
t_o	QGSJetII	53.06 (0.05)	-28.74 (0.12)	-275.93 (1.18)
	Sibyll2.1	60.48 (0.07)	-38.48 (0.13)	-402.80 (1.22)
σ	QGSJetII	-0.26 (0.06)	-5.63 (0.21)	31.68 (3.38)
	Sibyll2.1	-1.09 (0.07)	-5.28 (0.19)	44.41 (1.54)
λ	QGSJetII	-2.68 (0.14)	-19.50 (0.43)	100.32 (2.63)
	Sibyll2.1	-2.61 (0.11)	-17.89 (0.14)	96.28 (1.76)

Table 1: Fitted coefficients (equation 3)- CONEX. All values in g/cm^2.

	Had. Model	C_1 ($\pm$ err)	C_2 ($\pm$ err)	C_3 ($\pm$ err)
t_o	QGSJetII	53.32 (0.30)	-29.47 (0.52)	-283.93 (5.62)
	Sibyll2.1	60.77 (0.23)	-38.88 (0.31)	-408.88 (4.67)
σ	QGSJetII	0.06 (0.002)	-5.06 (0.17)	35.99 (3.21)
	Sibyll2.1	-0.56 (0.08)	-4.70 (0.21)	44.01 (2.03)
λ	QGSJetII	-1.73 (0.15)	-20.63 (0.34)	82.69 (3.54)
	Sibyll2.1	-2.49 (0.22)	-19.54 (0.34)	96.04 (3.46)

Table 2: Fitted coefficients (equation 3) - CORSIKA. All values in g/cm^2.

5. Conclusion

We have studied the simulation programs CORSIKA and CONEX with the hadronic interaction models Sibyll2.1 and QGSJetII. We have shown that the $\langle X_{\text{max}} \rangle$ and the RMS(X_{max}) depend slightly on the combination of program and hadronic interaction model chosen. It is widely known that $\langle X_{\text{max}} \rangle$ and RMS(X_{max}) predicted by Sibyll2.1 and

QGSJETII are different mainly due to the different extrapolations of the hadronic interaction properties to the highest energies. We have quantified here the differences between CORSIKA and CONEX by predicting the $\langle X_{\max} \rangle$ and the RMS($X_{\max}$) using the same hadronic interaction model. These differences are small, but should be considered as systematic uncertainties of the model predictions.

Figure 13 shows the evolution of the $\langle X_{\max} \rangle$ and RMS($X_{\max}$) with energy. No clear dependency of the difference between CORSIKA and CONEX with energy or primary particle type was seen. When using QGSJETII or SIBYLL2.1, CORSIKA and CONEX predict the $\langle X_{\max} \rangle$ with a difference smaller than 7 g/cm^2, and the RMS($X_{\max}$) with a difference smaller than 5 g/cm^2. The differences in the slopes of a linear fit to the evolution of the $\langle X_{\max} \rangle$ and RMS($X_{\max}$) with energy for CORSIKA and CONEX are quite small (< 3 %).

No assumption is made here for the cause of these differences. An investigation for the possible cause could be done, but in the meanwhile these differences between the programs should be considered as systematics error in the analysis of the $\langle X_{\max} \rangle$ and RMS($X_{\max}$) when one tries to infer the composition abundance. Table 3 shows the suggested systematic uncertainties for the model predictions. Maximum values for the systematic uncertainties can be extracted from figures 4e, 5e, 6e and 7e.

| Hadronic Model | Mass (A) | systematic uncertainty suggested for the model predictions | | |
		$\langle X_{\max} \rangle$ g/cm^2	RMS($X_{\max}$) g/cm^2	Elongation rate g/cm^2 per energy decade
SIBYLL2.1	1	$2.57 - 1.05 \times log_{10}(E/EeV)$	$-4.58 - 0.66 \times log_{10}(E/EeV)$	< 1.30
	55	$2.57 - 0.09 \times log_{10}(E/EeV)$	$-7.78 - 0.52 \times log_{10}(E/EeV)$	< 0.08
QGSJETII	1	$3.73 - 0.31 \times log_{10}(E/EeV)$	$-3.82 - 0.29 \times log_{10}(E/EeV)$	< 0.20
	55	$5.13 - 0.70 \times log_{10}(E/EeV)$	$-7.38 - 0.30 \times log_{10}(E/EeV)$	< 0.60

Table 3: Systematic uncertainties suggested for the model predictions.

Section 4 shows the parametrization of the $X_{\max}$ distributions as a function of energy and mass. The curves shown there can be used to estimate the first and second moments of the $X_{\max}$ distribution from abundance calculations based on astrophysical arguments. As an example of the usage of this parametrization we have taken the astrophysical models developed by Berezinsky et al. [32] (Model 3) and Allard et al. [11] (Model A) and used our paremetrization to transform the abundance curves predicted by the models into a $X_{\max}$ distribution. Figure 15 shows a $X_{\max}$ distributions predicted by the models in comparison to the data measured by the Pierre Auger Observatory [33]. We have convolved the model predictions with a Gaussian detector resolution of 20 g/cm^2. The utility of the parametrization is such that the models can be compared to the $X_{\max}$ distribution instead of only the $\langle X_{\max} \rangle$ and RMS($X_{\max}$).

6. Acknowledgments

[1] The Pierre Auger Collaboration, Observation of the suppression of the flux of cosmic rays above 4x10^{19} eV, Phys. Rev. Lett. 101 (2008) 061101.
[2] High Resolution Fly´s Eye Collaboration, First observation of the Greisen-Zatsepin-Kuzmin suppression, Phys. Rev. Lett. 100 (10) (2008) 101101.
[3] The Pierre Auger Collaboration, Measurement of the depth of maximum of extensive air showers above 10^{18} eV, Phys. Rev. Lett. 104.
[4] D. Bird, S. Corbat, H. Dai, B. Dawson, J. Elbert, T. Gaisser, K. Green, M. Huang, D. Kieda, S. Ko, C. Larsen, E. Loh, M. Luo, M. Salamon, D. Smith, P. Sokolsky, P. Sommers, T. Stanev, J. Tang, S. Thomas, S. Tilav, Evidence for correlated changes in the spectrum and composition of cosmic rays at extremely high energies, Phys. Rev. Lett. 71 (21) (1993) 3401–3404.
[5] Yuchiro Tameda for the TA Collaboration, Proc. 32th Int. Cosmic Ray Conference (2011) HE1.3.
[6] S.P.Knurenko, A. Sabourov, Proc. 32th Int. Cosmic Ray Conference (2011) HE1.3.
[7] The JEM-EUSO Collaboration, arXiv:1204.5065v1.
[8] W. Heitler, The Quantum Theory of Radiation, Third Edition, Oxford University Press, 1954.
[9] J. Matthews, A Heitler model of extensive air showers, Astroparticle Physics 22 (2005) 387 – 397.
[10] J. Knapp, D. Heck, S. Sciutto, M. Dova, M. Risse, Extensive air shower simulations at the highest energies, Astroparticle Physics 19 (1) (2003) 77–99.

[11] D. Allard, N. G. Busca, G. Decerprit, A. V. Olinto, E. Parizot, Implications of the cosmic ray spectrum for the mass composition at the highest energies, Journal of Cosmology and Astroparticle Physics 2008 (10) (2008) 033.

[12] Gopal-Krishna, P. L. Biermann, V. de Souza, P. J. Wiita, Ultra-high-energy cosmic rays from centaurus a: Jet interaction with gaseous shells, The Astrophysical Journal Letters 720 (2) (2010) L155.

[13] V. Berezinsky, A. Gazizov, S. Grigorieva, On astrophysical solution to ultrahigh energy cosmic rays, Phys. Rev. D 74 (2006) 043005. doi:10.1103/PhysRevD.74.043005.

[14] A. Hillas, astro-ph:0607109.

[15] T. Bergmann, R. Engel, D. Heck, N. Kalmykov, S. Ostapchenko, T. Pierog, T. Thouw, K. Werner, One-dimensional hybrid approach to extensive air shower simulation, Astroparticle Physics 26 (6) (2007) 420–432.

[16] T. Pierog, M. Alekseeva, T. Bergmann, V. Chernatkin, R. Engel, D. Heck, N. Kalmykov, J. Moyon, S. Ostapchenko, T. Thouw, K. Werner, First results of fast one-dimensional hybrid simulation of EAS using conex, Nuclear Physics B - Proceedings Supplements 151 (1) (2006) 159–162.

[17] D. Heck, J. Knapp, J. Capdevielle, G. Schatz, T. Thouw, A Monte-Carlo code to simulate extensive air showers - report FZKA 6019, Tech. rep., Forschungszentrum Karlsruhe (1998).

[18] A. Hillas, Proc. 17th Int. Cosmic Ray Conference 8 (1981) 193.

[19] A. Hillas, Proc. 19th Int. Cosmic Ray Conference 1 (1985) 155.

[20] S. Ostapchenko, On the re-summation of enhanced pomeron diagrams, Physics Letters B 636 (1) (2006) 40–45.

[21] S. Ostapchenko, Nonlinear screening effects in high energy hadronic interactions, Physical Review D 74 (1).

[22] R. Fletcher, T. Gaisser, P. Lipari, T. Stanev, Sibyll: An event generator for simulation of high energy cosmic ray cascades, Physical Review D 50 (9) (1994) 5710–5731.

[23] H. Fesefeldt, Tech. rep., RWTH Aachen, report PITHA-85/02 (1985).

[24] T. K. Gaisser, A.M. Hillas, Proc. 15th Int. Cosmic Ray Conference 8 (1977) 353.

[25] Private Communication: T. Pierog.

[26] K.-H. Kampert, M. Unger, Measurements of the cosmic ray composition with air shower experiments, Astroparticle Physics 35 (10) (2012) 660 – 678. doi:10.1016/j.astropartphys.2012.02.004.

[27] J. Linsley, Proc. 15th Int. Cosmic Ray Conference 12 (1977) 89.

[28] T. K. Gaisser, T. J. K. McComb, K. E. Turver, Proc. 16th Int. Cosmic Ray Conference 9 (1979) 258.

[29] J. Linsley, A. Watson, Validity of scaling to 10^{20} eV and High-Energy Cosmic-Ray composition, Phys. Rev. Lett. 46 (7) (1981) 459–463.

[30] D. Heck, The influence of hadronic interaction models on simulated air-showers:a phenomenological comparison. URL www-ik.fzk.de/corsika/corsika-school2008/talks

[31] Private Communication: P. Facal.

[32] V. Berezinsky, S. Grigorieva, B. Hnatyk, Extragalactic UHE proton spectrum and prediction for iron-nuclei flux at 10^8 - 10^9 GeV, Astroparticle Physics 21 (6) (2004) 617 – 625. doi:10.1016/j.astropartphys.2004.06.004.

[33] The Pierre Auger Collaboration, The Pierre Auger Observatory II: Studies of cosmic ray composition and hadronic interaction models, Proc. 32th Int. Cosmic Ray Conference , arXiv:1107.4804.

(a) THIN = 10^{-5} (b) THIN = 10^{-6} (c) THIN = 10^{-7}
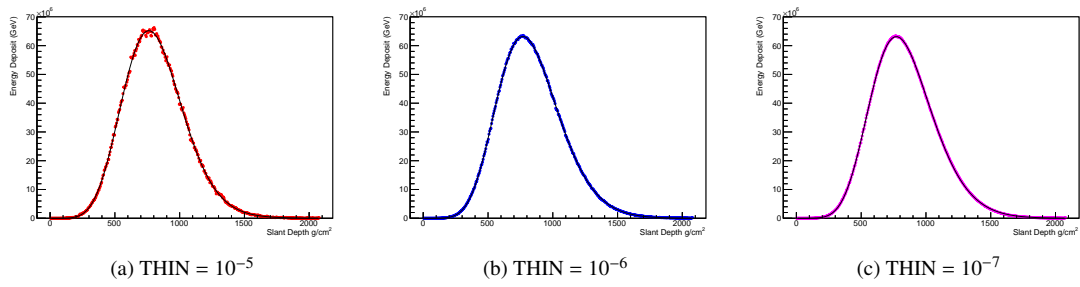
Figure 1: Longitudinal development of proton showers with energy 10^{19} eV for different thinning factors. Each figure shows the development of one shower.Sibyll2.1 was used for this study.
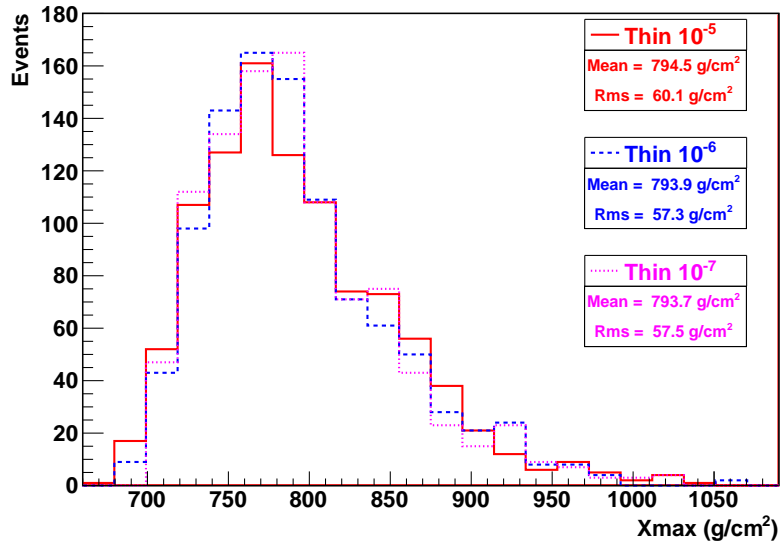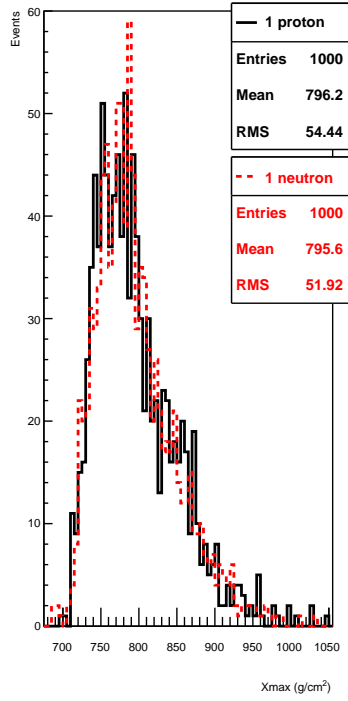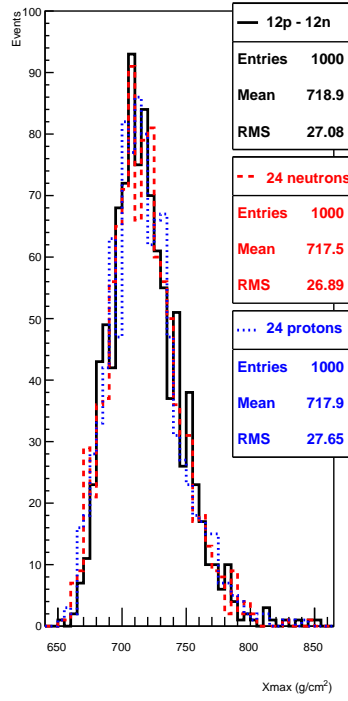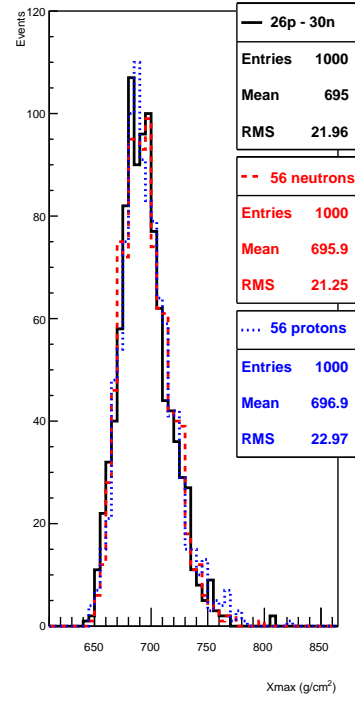

Figure 2: X_{max} distribution for 1000 proton showers with 10^{19} eV simulated with different thinning factors. Sibyll2.1 was used for this study.
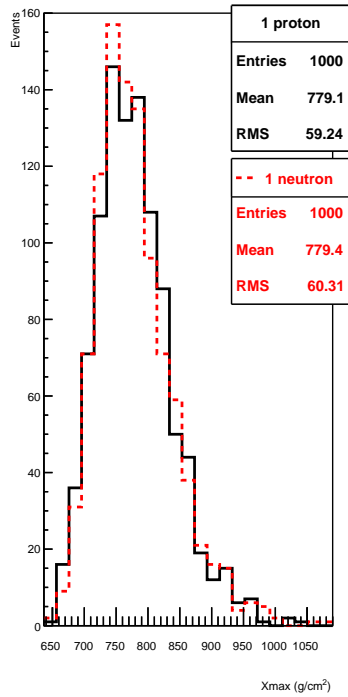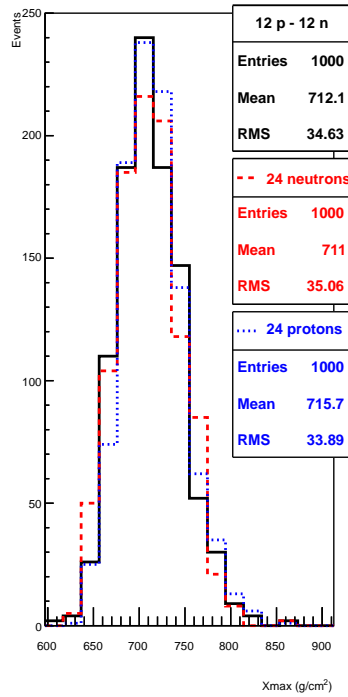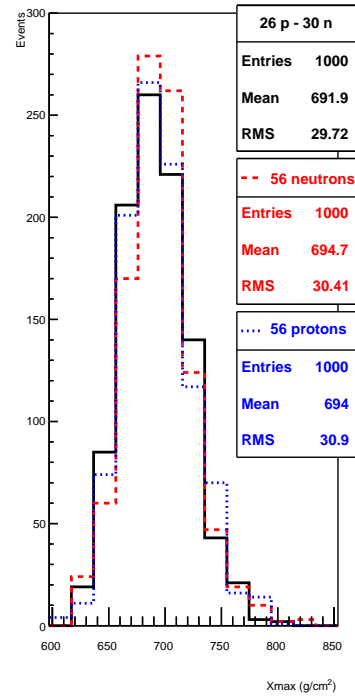
(a) Atomic Weight: 1 - SIBYLL.

(b) Atomic Weight: 24 - SIBYLL.

(c) Atomic Weight: 56 - SIBYLL.

(d) Atomic Weight: 1 - QGSJETII.

(e) Atomic Weight: 24 - QGSJETII

(f) Atomic Weight: 56 - QGSJETII

9

Figure 3: Study on the $X_{\max}$ distribution for nuclei with different nucleon constitutions.
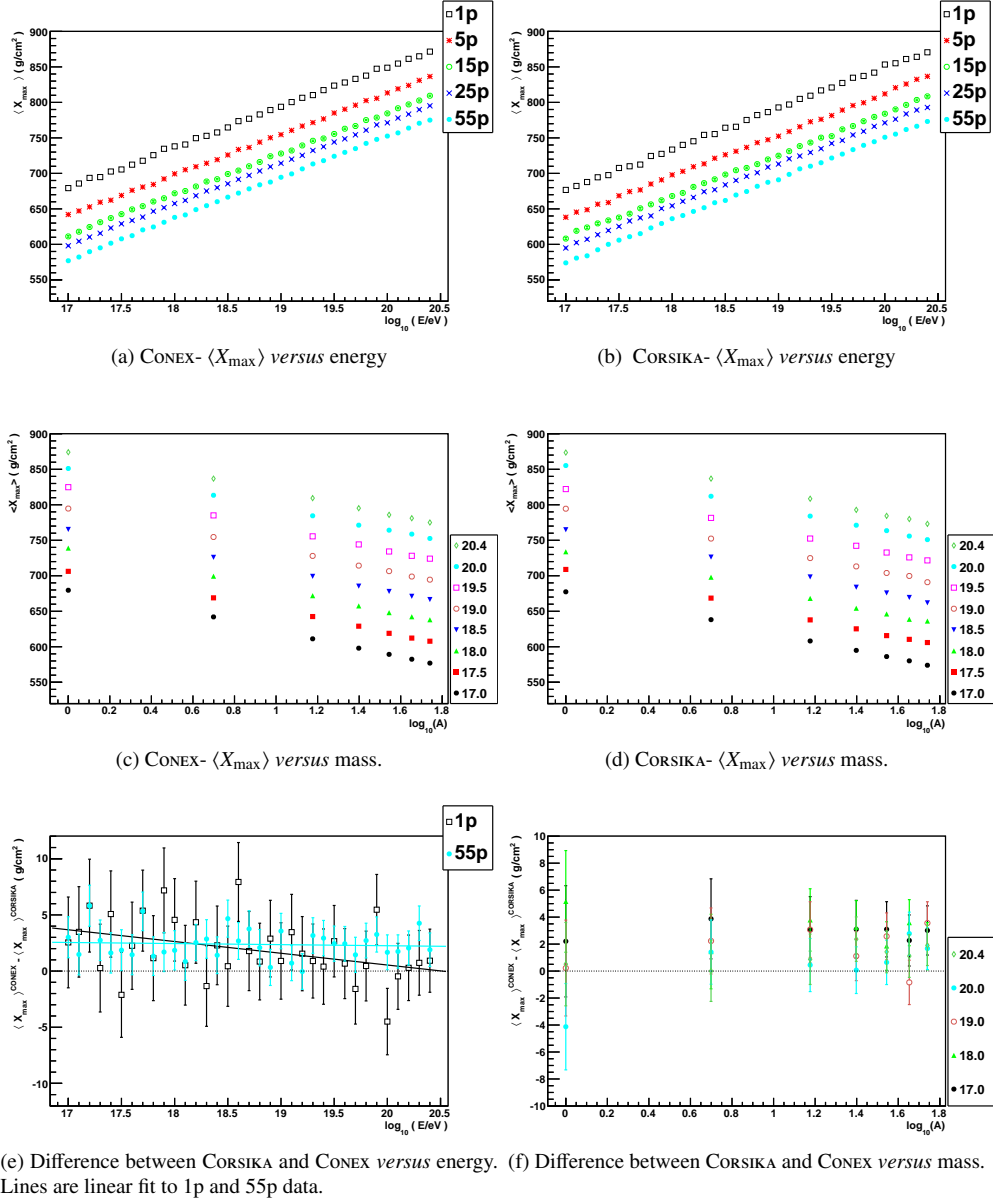
(a) Conex- $\langle X_{max} \rangle$ *versus* energy

(b) Corsika- $\langle X_{max} \rangle$ *versus* energy

(c) Conex- $\langle X_{max} \rangle$ *versus* mass.

(d) Corsika- $\langle X_{max} \rangle$ *versus* mass.

(e) Difference between Corsika and Conex *versus* energy. (f) Difference between Corsika and Conex *versus* mass.
Lines are linear fit to 1p and 55p data.

Figure 4: $\langle X_{max} \rangle$ as a function of energy and mass as calculated by Corsika and Conex using Sibyll2.1. Showers have been simulated with primary energy ranging from $10^{17.0}$ to $10^{20.4}$ eV in steps of $\log_{10}(E/eV) = 0.1$ and primary nuclei types with mass: 1, 5, 15, 25, 35, 45 and 55. A set of 1000 showers has been simulated for each combination. Not all energies and primaries are shown for clarity.
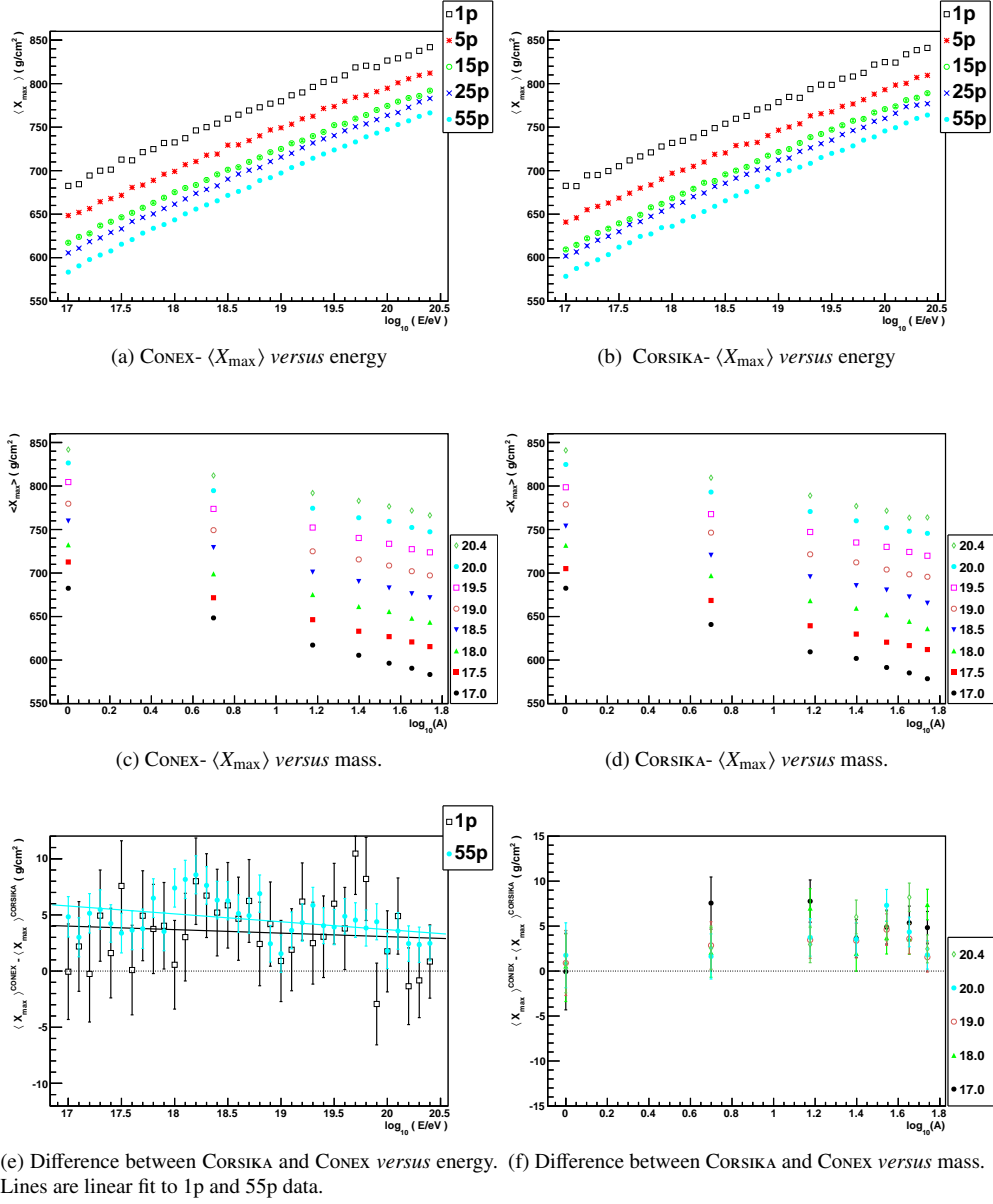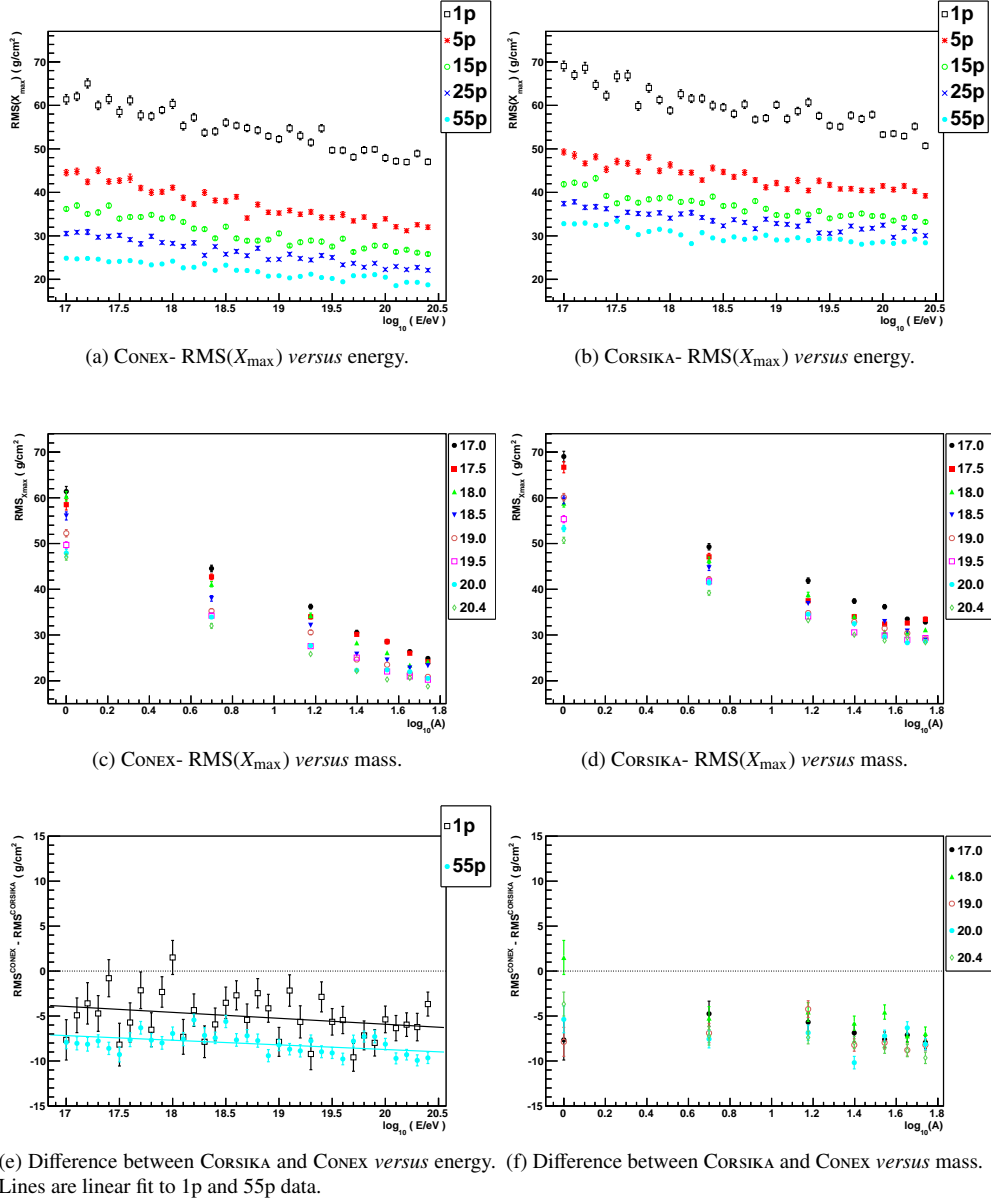
10

(a) CONEX- $\langle X_{max} \rangle$ *versus* energy

(b) CORSIKA- $\langle X_{max} \rangle$ *versus* energy

(c) CONEX- $\langle X_{max} \rangle$ *versus* mass.

(d) CORSIKA- $\langle X_{max} \rangle$ *versus* mass.

(e) Difference between CORSIKA and CONEX *versus* energy. (f) Difference between CORSIKA and CONEX *versus* mass.
Lines are linear fit to 1p and 55p data.

Figure 5: $\langle X_{max} \rangle$ as a function of energy and mass as calculated by CORSIKA and CONEX using QGSJETII. Showers have been simulated with primary energy ranging from $10^{17.0}$ to $10^{20.4}$ eV in steps of $\log_{10}(E/eV) = 0.1$ and primary nuclei types with mass: 1, 5, 15, 25, 35, 45 and 55. A set of 1000 showers has been simulated for each combination. Not all energies and primaries are shown for clarity.
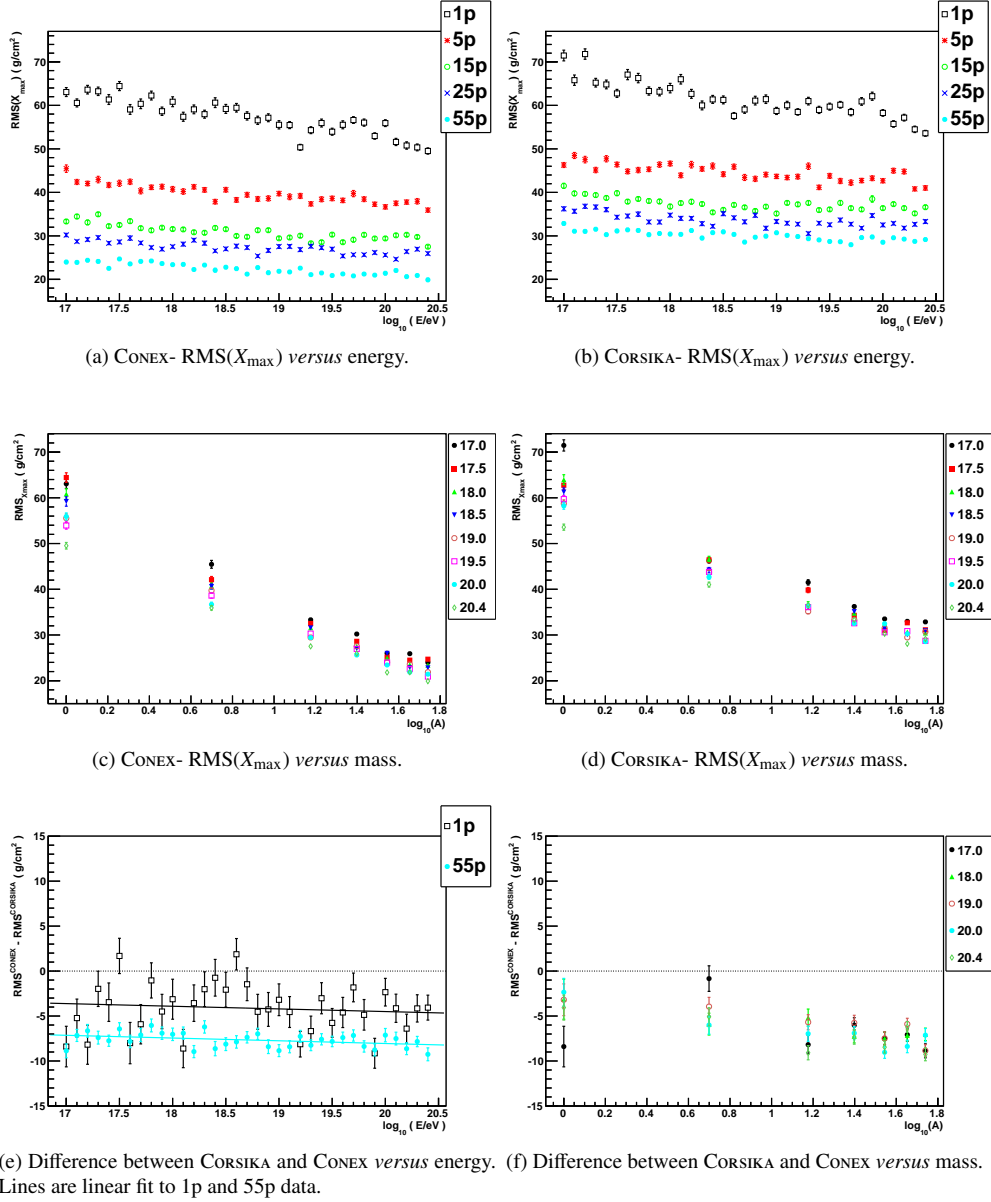
11

(a) Conex- RMS(X_{max}) *versus* energy.

(b) Corsika- RMS(X_{max}) *versus* energy.

(c) Conex- RMS(X_{max}) *versus* mass.

(d) Corsika- RMS(X_{max}) *versus* mass.

(e) Difference between Corsika and Conex *versus* energy. Lines are linear fit to 1p and 55p data.

(f) Difference between Corsika and Conex *versus* mass.

Figure 6: RMS(X_{max}) as a function of energy and mass as calculated by Corsika and Conex using Sibyll2.1. Showers have been simulated with primary energy ranging from $10^{17.0}$ to $10^{20.4}$ eV in steps of $\log_{10}(E/eV) = 0.1$ and primary nuclei types with mass: 1, 5, 15, 25, 35, 45 and 55. A set of 1000 showers has been simulated for each combination. Not all energies and primaries are shown for clarity.

(a) Conex- RMS(X_{max}) *versus* energy.

(b) Corsika- RMS(X_{max}) *versus* energy.

(c) Conex- RMS(X_{max}) *versus* mass.

(d) Corsika- RMS(X_{max}) *versus* mass.

(e) Difference between Corsika and Conex *versus* energy.
Lines are linear fit to 1p and 55p data.

(f) Difference between Corsika and Conex *versus* mass.

Figure 7: RMS(X_{max}) as a function of energy and mass as calculated by Corsika and Conex using QGSJetII. Showers have been simulated with primary energy ranging from $10^{17.0}$ to $10^{20.4}$ eV in steps of $\log_{10}(E/eV) = 0.1$ and primary nuclei types with mass: 1, 5, 15, 25, 35, 45 and 55. A set of 1000 showers has been simulated for each combination. Not all energies and primaries are shown for clarity.

13
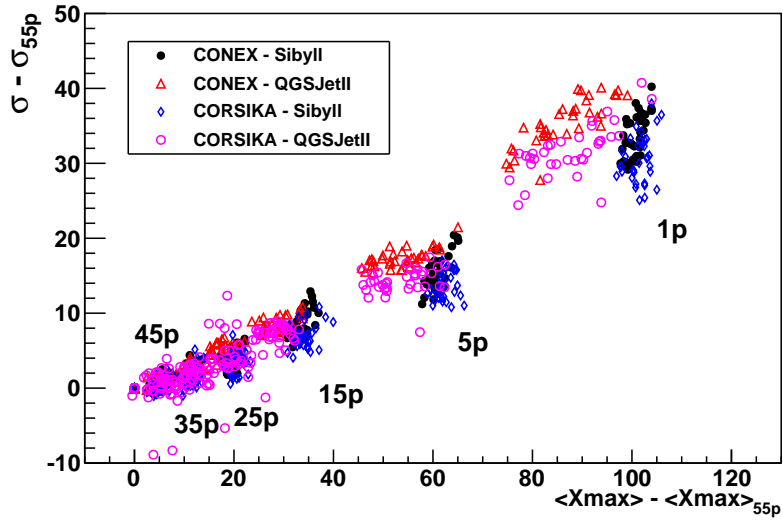
Figure 8: RMS(X_max) *versus* $\langle X_\mathrm{max} \rangle$ for all primary particles used in this work. The corresponding RMS(X_max) and $\langle X_\mathrm{max} \rangle$ for a nuclei with mass 55 has been taken as reference. Each blob corresponds to the $\langle X_\mathrm{max} \rangle$ and RMS(X_max) predictions for one primary particle at different energies.

(a) Slope of $\langle X_\mathrm{max} \rangle$ *versus* mass - Sibyll2.1.

(b) Slope of $\langle X_\mathrm{max} \rangle$ *versus* mass - QGSJetII.

(c) Slope of RMS(X_max) *versus* mass - Sibyll2.1.

(d) Slope of RMS(X_max) *versus* mass - QGSJetII.
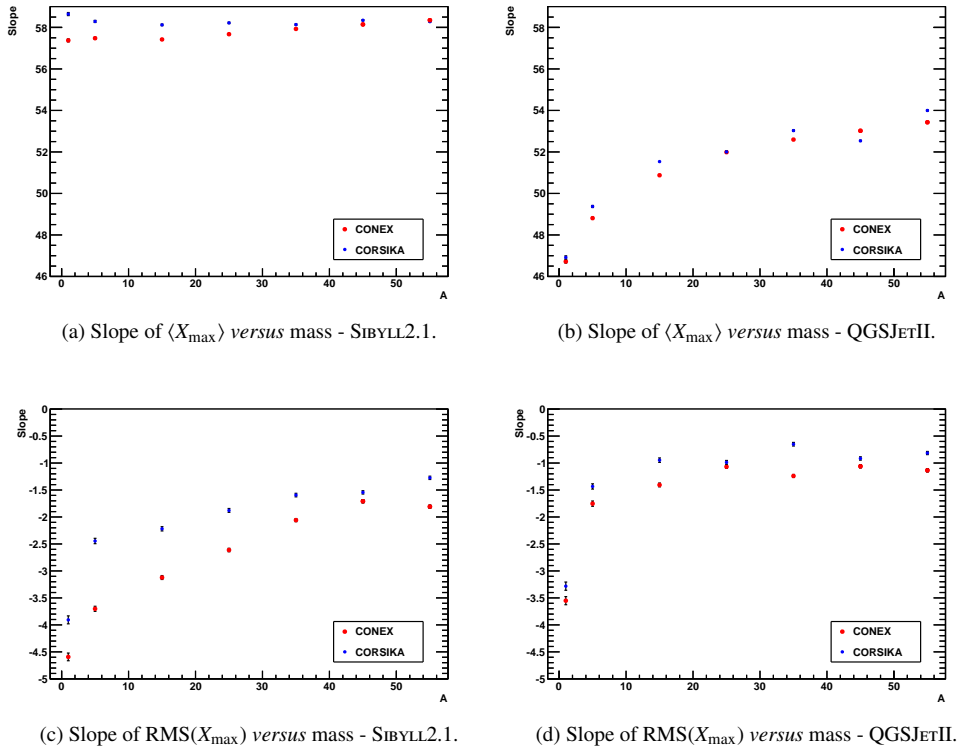
Figure 9: Slope Analysis. Slope of a straight line fit to the variation of $\langle X_\mathrm{max} \rangle$ and RMS(X_max) with energy (plotted as a function of mass). Slope in units of g/cm^2/eV.

14

(a) t_0 (b) σ (c) λ
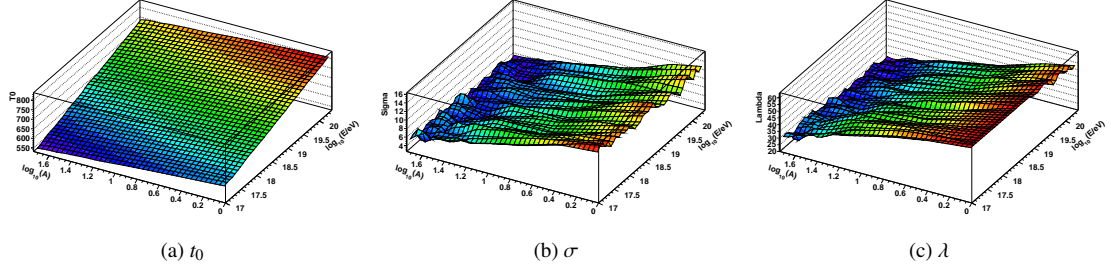
Figure 10: Parametrization of the $X_{\max}$ distribution. CONEX- SIBYLL2.1. These figures show the general behavior of the three parameters used to describe the $X_{\max}$ distributions as a function of energy and mass.
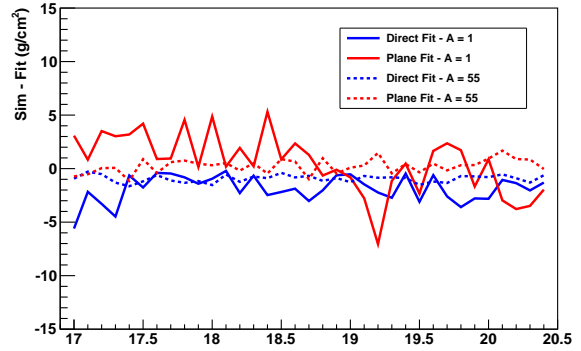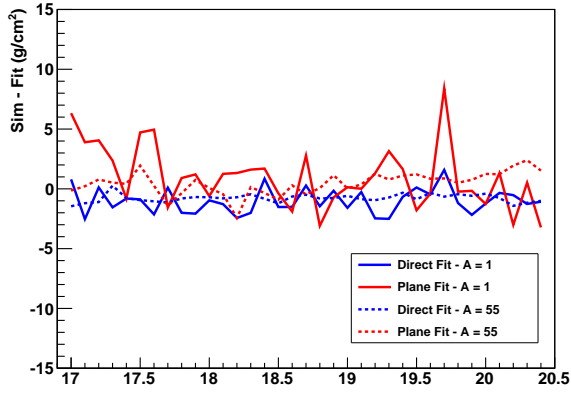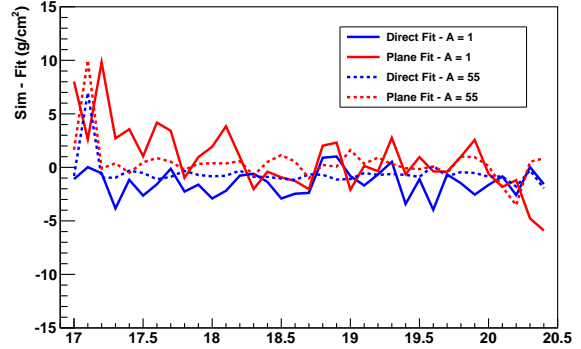

(a) CONEX- SIBYLL2.1

(b) CONEX- QGSJETII

(c) CORSIKA- SIBYLL2.1
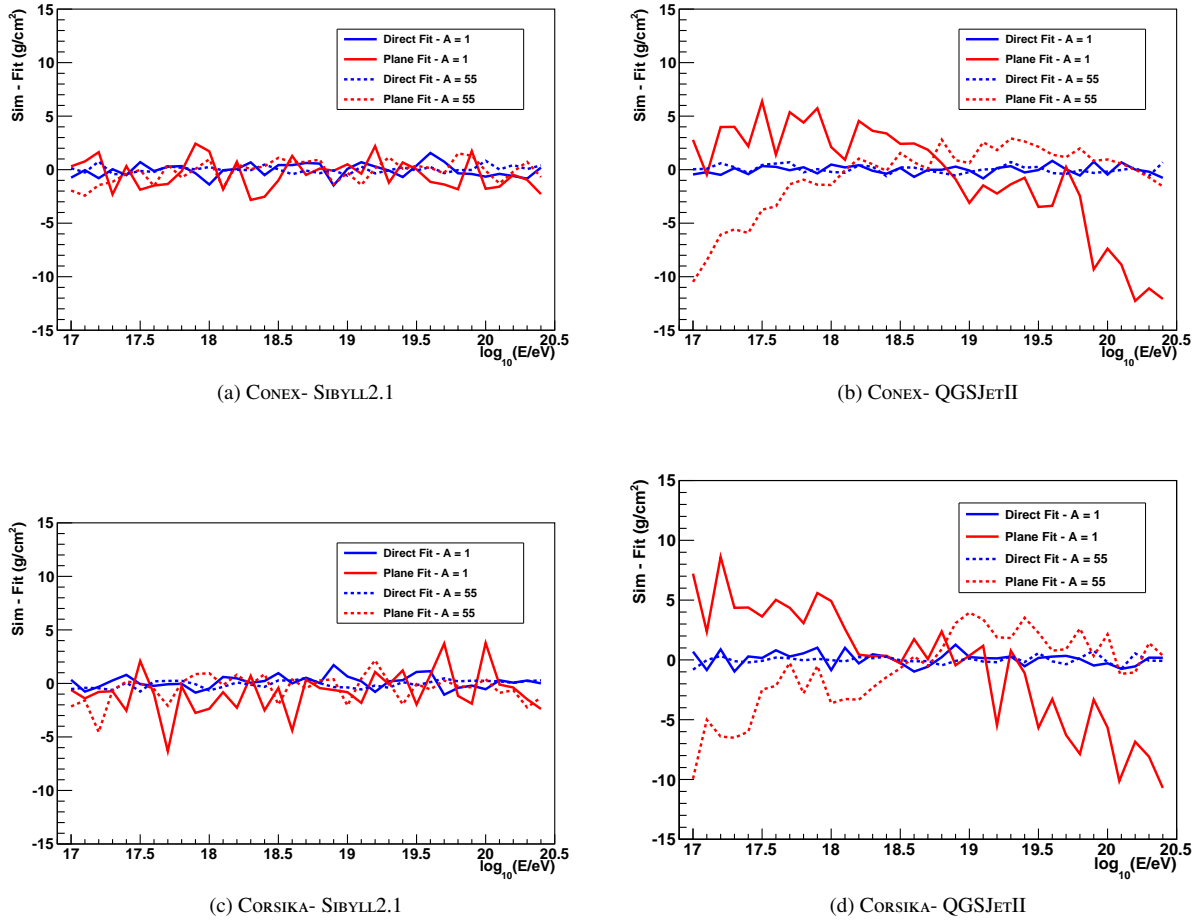
(d) CORSIKA- QGSJETII

Figure 11: Differences in $\langle X_{\max} \rangle$ *versus* energy. Comparison between the simulation, the direct fit of the $X_{\max}$ distribution using equation 2 and the calculation using equation 3 and table 1

15
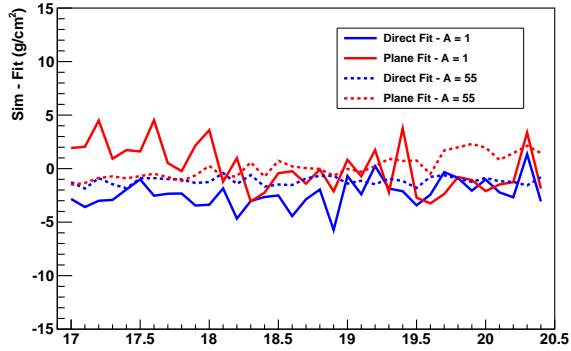
(a) CONEX- SIBYLL2.1

(b) CONEX- QGSJETII

(c) CORSIKA- SIBYLL2.1

(d) CORSIKA- QGSJETII

Figure 12: Differences in RMS(X_{max}) *versus* energy. Comparison between the simulation, the direct fit of the X_{max} distribution using equation 2 and the calculation using equation 3 and table 1
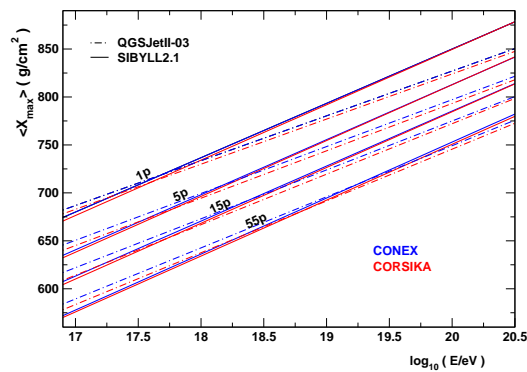
(a) $\langle X_{\mathrm{max}} \rangle$.
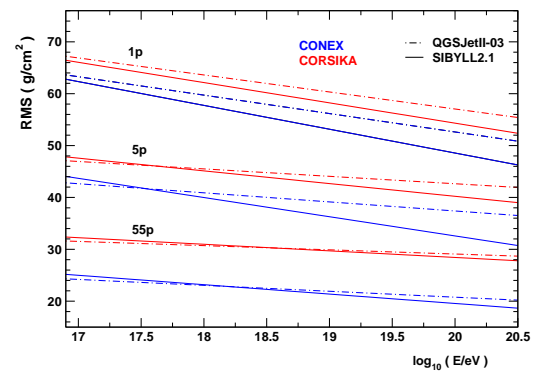
(b) RMS(X_{max}).

Figure 13: Comparison of $\langle X_{\mathrm{max}} \rangle$ and RMS(X_{max}) for CORSIKA and CONEX as a function of energy.

(a) A = 1 - 10^{18} eV.
(b) A = 1 - 10^{19} eV.
(c) A = 1 - 10^{20} eV.
(d) A = 55 - 10^{18} eV.
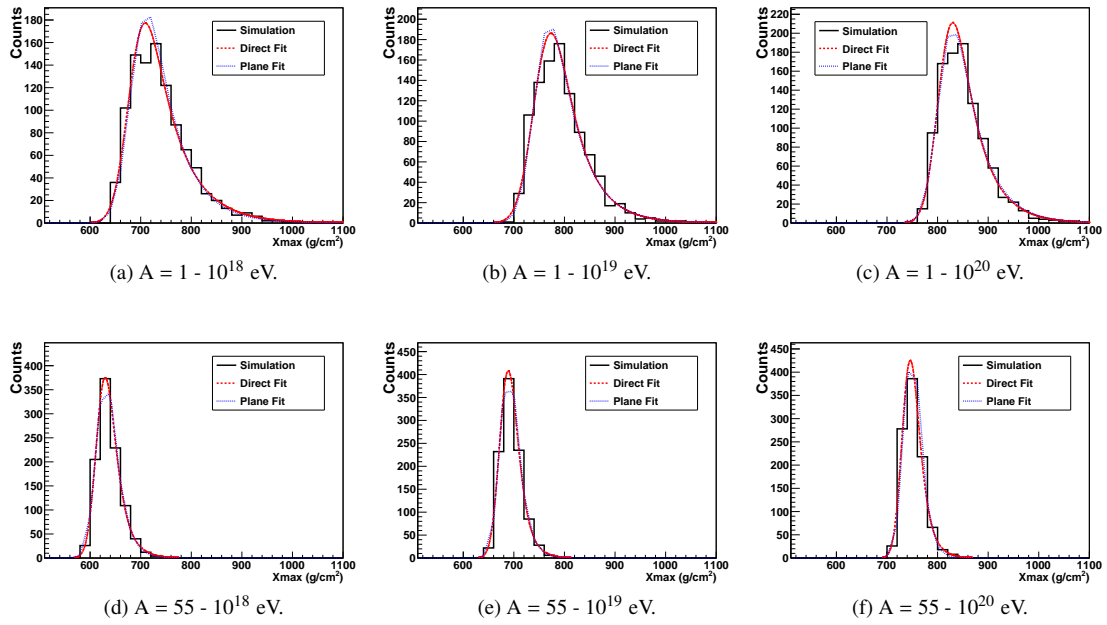(e) A = 55 - 10^{19} eV.
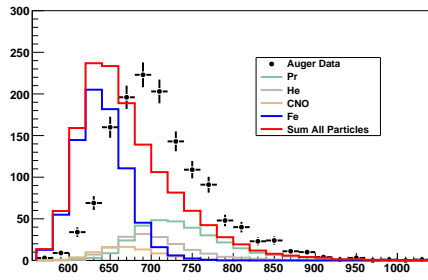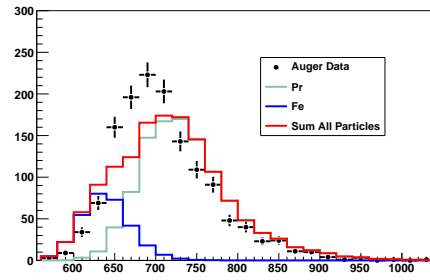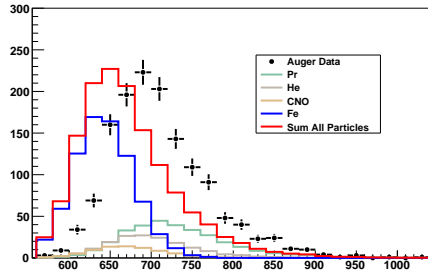(f) A = 55 - 10^{20} eV.

Figure 14: Simulated X_{max} distribution fitted by a Gaussian convoluted with an exponential (equation 2). In this example we show showers simulated with Conex and Sibyll2.1. Full line shows the X_{max} distribution and dashed line the fit of equation 2.
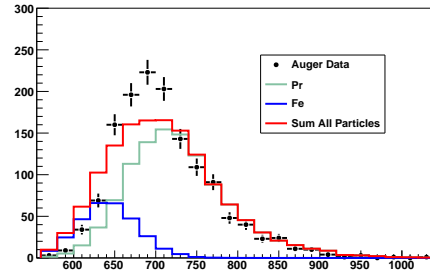
17

(a) Allard et al. - Conex- Sibyll2.1.

(b) Berezinsky et al. - Conex- Sibyll2.1.

(c) Allard et al. - Corsika- QGSJetII.

(d) Berezinsky et al. - Corsika- QGSJetII.

Figure 15: X_{max} distributions. Data measured by the Pierre Auger Observatory with energy $10^{18.0} < E < 10^{18.1}$ eV [33]. Astrophysical models extracted from [13, 11]. The models have been calculated at $E = 10^{18.05}$ eV. The curves have been calculated using the parametrizations proposed above.

18